Wrench Analysis of Cable-Suspended Parallel Robots Actuated by Quadrotors UAVs

Julian Benedict Czapalay Erskine, Abdelhamid Chriette, Stéphane Caro

Wrench Analysis of Cable-Suspended Parallel Robots Actuated by Quadrotors UAVs

Julian Erskine
École Centrale de Nantes, LS2N *
Email: Julian.Erskine@ls2n.fr

Abdelhamid Chriette
École Centrale de Nantes, LS2N
Email: Abdelhamid.Chriette@ls2n.fr

Stéphane Caro†
Centre National de la Recherche Scientifique, LS2N
Email: Stephane.Caro@ls2n.fr

Aerial cable towed systems (ACTSs) can be created by joining unmanned aerial vehicles (UAVs) to a payload to extend the capabilities of the system beyond those of an individual UAV. This paper describes a systematic method for evaluating the available wrench set and the robustness of equilibrium of ACTSs by adapting wrench analysis techniques used in traditional cable-driven parallel robots to account for the constraints of quadrotor actuation and dynamics. Case studies and experimental results are provided to demonstrate the analysis of different classes of ACTSs, as a means of evaluating the design and operating configurations.

Keywords: *Quadrotor, Cable-Driven Parallel Robot, Wrench Feasibility, Capacity Margin, Aerial Manipulation*

1 INTRODUCTION

Aerial cable towed systems (ACTSs) are a class of aerial manipulator that is gaining interest as a means of payload transportation and manipulation. Currently most ACTSs are slung loads from helicopters for the purpose of military or civilian logistics, but the recent increase in the commercialization of unmanned aerial vehicles (UAVs) due to improved onboard sensing and computation, and higher energy density batteries has opened the commercial possibility of using many small UAVs to collaborate towards single tasks [1–3]. The use of multiple small UAVs compared to a single larger one is desirable from a safety and redundancy standpoint, as well as allowing for greater reactivity of the system to excitations due to the greater agility of small UAVs [4]. Many types of UAVs exist, however much of the current research including this paper is focused on quadrotors due to their high payload to weight ratio, versatile control, and simple mechanical design [5].

ACTSs are composed of aerial vehicles connected to either a rigid body payload or to a point mass through cables.

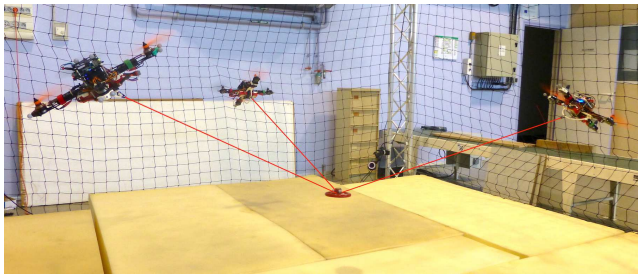

Fig. 1: Prototype ACTS developed at LS2N

Systems of multiple UAVs give greater versatility in the control of the payload and expand the available task set of the system, as well as delivering an attractive degree of modularity [6, 7]. Studies in which a single UAV with a slung load as in [8] found that complex control and trajectory generation was required to avoid payload oscillations, a problem intuitively solved by constraining the load through more cables.

Much of the current research into ACTSs is focused on designing trajectory tracking controllers for the suspended body. In [9], differential flatness is used to generate feasible trajectories for the system. The authors of [10] use control methods adapted from cable-driven parallel robots (CDPRs) to ensure stability and trajectory convergence, while in [11], a linear quadratic regulator is used to control the robot. In [12], a novel ACTS is presented and uses RRT graphs to determine feasible payload trajectories. A subject of great interest currently in the ACTS field is the implementation of decentralized control where the payload is transported by the collective action of multiple quadrotors without explicit communication between each agent. This has been studied for rigid connections [2], and for cable attachments using onboard camera [4] or using either observer or sensor derived tension sensing [13, 14] where the stability is shown to relate to the internal forces in the body being transported. In all these works the wrench feasibility and stability of the

*Laboratoire des Sciences du Numérique de Nantes (LS2N), UMR 6004, 1 Rue de la Noë, 44321 Nantes, France
†Corresponding author

ACTS is considered, but to the authors' best knowledge there is no systematic quantification of the degree of wrench feasibility nor generic methodology for mapping the extensive wrench set in task space.

There are strong similarities between ACTSs and CDPRs, indeed an ACTS can be considered as a CDPR with moving pulley anchor points. Wrench capabilities have been an important topic of research for CDPRs, playing an important role in their design, workspace analysis, and trajectory generation [15–18]. The link between CDPRs and ACTSs has been investigated by using tension distribution algorithms for the purposes of control and stability [10, 19]. In [20], the degree of wrench inclusion is used as a performance index for CDPRs. Despite the similitudes of the two types of systems, there are differences in the modelling of the available wrench set due to the actuation limits of quadrotors. The purpose of this paper is therefore to develop a broadly applicable means of evaluating the available wrench set of ACTSs, with possible applications in design, motion planning, and for evaluating the robustness of equilibrium.

Section 2 of this paper describes the parameterization of ACTSs. In section 3, the equilibrium conditions of the platform and quadrotors are formalized. The methodology used for calculating the available wrench set of the ACTS is shown in section 4 for a simple planar system. Several quasi-static case studies are presented in section 5, showing the application for more complex planar and spatial systems. Experimental validation is presented in section 6 and section 7 presents the effects of dynamics on the wrench analysis.

2 GEOMETRIC PARAMETERIZATION

To formulate a general methodology, a parameterization of the ACTS allowing for design variability is important. In this case, an ACTS with n quadrotors, m cables, and a d DOF payload is considered. From a practical perspective, it is assumed that the pose of the quadrotors and payload are known with respect to an inertial frame $\mathcal{F}_0$ at origin O. The platform frame $\mathcal{F}_p$ is placed at the center of mass and inertia of the payload denoted as point P. The j^{th} cable of length l_j connects at point B_j to the payload at one end and to the i^{th} quadrotor at point A_i on the other end, with A_i being the center of mass and geometric center of the quadrotor. Each quadrotor has a frame $\mathcal{F}_i$ at point A_i, with the z-axis normal to the plane of the rotors.

The payload position vector $\mathbf{x}_p = \overrightarrow{OP}$ is expressed in $\mathcal{F}_0$, and in the case of rigid body payloads the rotation from $\mathcal{F}_0$ to $\mathcal{F}_p$ is given by the rotation matrix $\mathbf{R}_p$. The position vector of the i^{th} quadrotor is expressed in $\mathcal{F}_0$ as $\mathbf{x}_i = \overrightarrow{OA_i}$ and the orientation by rotation matrix $\mathbf{R}_i$. The point B_j is defined in $\mathcal{F}_p$ as $\mathbf{b}_j = \overrightarrow{PB_j}$. The configuration of the ACTS is described by the set of cable vectors $\mathbf{u}_{1\ldots,m}$, with $\mathbf{u}_j$ being the unit vector along $\overrightarrow{B_jA_i}$ in $\mathcal{F}_0$. As a function of measured states, the cable vector $\mathbf{u}_j$ is given by Eqn. (1).

$$l_j\mathbf{u}_j = \mathbf{x}_i - \mathbf{x}_p - \mathbf{R}_p\mathbf{b}_j \tag{1}$$

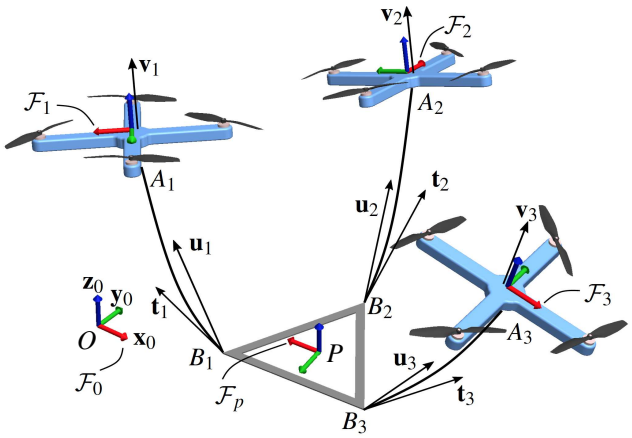

Fig. 2: Parameterization of an Aerial Cable Towed System with a rigid platform. This general representation shows curved cables to distinguish them from rigid links, but as the cable mass decreases they approach straight lines and $\mathbf{t}_i$ becomes parallel to $\mathbf{u}_i$.

3 EQUILIBRIUM CONDITIONS OF ACTS

This paper describes the available wrench set of an ACTS as a function of the thrust capabilities of each quadrotor, as well as their configurations relative to the payload, and their desired acceleration. It is considered that a known external wrench $\mathbf{w}_e = [\mathbf{f}_e^T \ \mathbf{m}_e^T]^T$ expressed in $\mathcal{F}_0$ acts on the platform. The equations of motions acting on the platform and on each quadrotor are expressed separately to determine the total external and internal forces, effectively dividing the systems into three components; the quadrotors, the platform, and the cables linking the two together.

3.1 Platform

Assumption 1: Cables are considered to be massless and inelastic. This means that the cables can be considered as straight lines, and as such the i^{th} cable tension vector can be defined as $\mathbf{t}_i = t_i\mathbf{u}_i$.

The wrenches on the payload are generated through the sum of m tension vectors and their corresponding moments, along with gravity acting at the center of mass. There are therefore $m+1$ constraining wrenches on the payload. In cases where the payload is considered a point mass, the moments generated by the cables are disregarded. As a result, the equations of motion of the platform expressed in frame $\mathcal{F}_0$ are as follows:

$$m_p\mathbf{g} + \sum_{j=1}^{m}(t_j\mathbf{u}_j) + \mathbf{f}_e = m_p\ddot{\mathbf{x}}_p \tag{2}$$

$$\sum_{j=1}^{m}(\mathbf{R}_p\mathbf{b}_j \times t_j\mathbf{u}_j) + \mathbf{m}_e = \mathbf{J}_p\dot{\boldsymbol{\omega}}_p + \boldsymbol{\omega}_p \times \mathbf{J}_p\boldsymbol{\omega}_p \tag{3}$$

where m_p is the mass of the platform, $\mathbf{g}$ is the gravitational vector $[0\,0\,-9.81]^T ms^{-2}$, and $\boldsymbol{\omega}_p$ is the angular velocity vector of the platform. Matrix $\mathbf{J}_p$ is the inertia tensor of the platform expressed in $\mathcal{F}_p$.

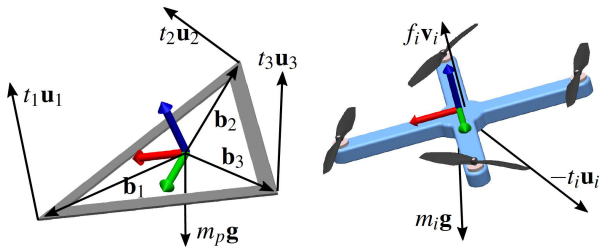

Fig. 3: Free body diagram of the platform and i^{th} quadrotor

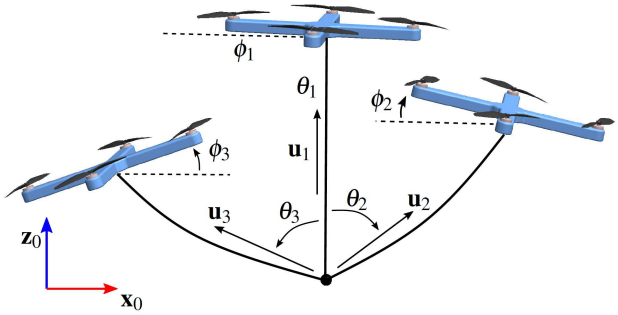

Fig. 4: A planar ACTS with three quadrotors, three cables, and a point mass payload

3.2 Quadrotors

The actuation wrench of the i^{th} quadrotor is expressed in $\mathcal{F}_i$ as ${}^i\mathbf{w}_i = [{}^i\mathbf{f}_i^T \ {}^i\boldsymbol{\tau}_i^T]^T$, where ${}^i\mathbf{f}_i$ is the thrust vector $[0\ 0\ f_i]^T$ and ${}^i\boldsymbol{\tau}_i$ is the moment vector $[\tau_{i,x}\ \tau_{i,y}\ \tau_{i,z}]^T$ [5]. The components of ${}^i\mathbf{w}_i$ take the form:

$$f_i = \sum_{i=1}^{i=4} C_F \omega_i^2 \tag{4a}$$

$$\tau_{x,i} = C_F r_i \left(\omega_1^2 - \omega_3^2\right) \tag{4b}$$

$$\tau_{y,i} = C_F r_i \left(\omega_2^2 - \omega_4^2\right) \tag{4c}$$

$$\tau_{z,i} = C_M \left(\omega_1^2 - \omega_2^2 + \omega_3^2 - \omega_4^2\right) \tag{4d}$$

where ω_i is the anguar velocity of the i^{th} propellor, r_i is the distance from the center of the i^{th} propellor to the quadrotor center of mass. C_F and C_M are the coefficients of thrust and drag of the propellors, respectively. It can be seen that a quadrotor exerts a thrust normal to the plane containing its rotors, and three independent moments about its center of inertia. This results in four degrees of actuation controlling the orientation of the unit vector $\mathbf{v}_i = \mathbf{R}_i[0\ 0\ 1]^T$, and the magnitude of the thrust f_i along $\mathbf{v}_i$.

Assumption 2: Cables pass through the center of mass of the quadrotor to which they are attached. This allows the assumption that the rotational dynamics of the quadrotor are fully decoupled from the cable tensions

The equations of motion of the i^{th} quadrotor expressed in $\mathcal{F}_0$ are written as:

$$f_i\mathbf{v}_i + m_i\mathbf{g} - \sum_{j=1}^{k} t_j\mathbf{u}_j = m_i\ddot{\mathbf{x}}_i \tag{5}$$

$$\boldsymbol{\tau}_i = \mathbf{J}_i\dot{\boldsymbol{\omega}}_i + \boldsymbol{\omega}_i \times \mathbf{J}_i\boldsymbol{\omega}_i \tag{6}$$

where $k \in [1,2]$ is the number of cables connected to the i^{th} quadrotor, m_i is the mass of the i^{th} quadrotor, and $\boldsymbol{\omega}_i$ is the angular velocity of the i^{th} quadrotor. Matrix $\mathbf{J}_i$ is the inertia tensor of the i^{th} quadrotor expressed in $\mathcal{F}_i$.

4 AVAILABLE WRENCH SET

With the ultimate goal of determining the available wrench set of an ACTS, the mapping of cable tension space used with CDPRs [20,21] is adapted to account for quadrotor constraints. The main difference between the CDPR and the ACTS available wrench sets is that CDPRs have a constant available tension set regardless of the state of the robot, so for any configuration of the CDPR the minimum and maximum available cable tensions are constant. Because a component of the actuation of the quadrotor is required to keep itself in the air, different configurations will result in variable tension spaces achievable by the ACTS, in turn affecting the set of available wrenches in task space. To this end, an extra mapping step is proposed to go from the thrust space of the quadrotors to the tension space of the cable system.

During the explanation of the available wrench set calculations, an example of a planar ACTS (Figure 4) composed of three quadrotors with a single cable each attached to a point mass will be used. It has the configuration $\mathcal{C} = [\theta_1\ \theta_2\ \theta_3] = [0\ \frac{\pi}{4}\ -\frac{7\pi}{18}] rad$, and a payload mass of $m_p = 4kg$. The quadrotors used have a mass of $m_i = 0.8kg$ and maximum thrust of $\bar{f}_i = 32N$. In a general case, there are n quadrotors, m cables, and a task space of dimension d, satisfying the following requirements:

$$1 \leq d \leq 6 \quad \text{and} \quad d \leq m \quad \text{and} \quad n \leq m \leq 2n$$

4.1 Thrust Space

As the i^{th} cable of this ACTS connects with the i^{th} quadrotor at $\mathbf{x}_i$ and can only transmit internal tensions, the thrust f_i is the only component of ${}^i\mathbf{w}_i$ that gets transmitted to the payload. Quadrotor i's thrust f_i is bounded by the strictly positive minimum thrust $\underline{f}_i$ required to maintain control of the quadrotor, and the maximum thrust $\bar{f}_i$ that the quadrotor can generate. The lower bound is of little significance to the wrench analysis, so long as $\ddot{\mathbf{x}}_i^T[0\ 0\ 1]^T > \mathbf{g}^T[0\ 0\ 1]^T$.

The upper bounds of the thrust space are simply the maximum thrust the quadrotors are able to generate. In the planar case study with three quadrotors, the thrust space is a 3-orthotope (Figure 5a). The thrust space $\mathcal{H}$ can be generalized for an arbitrary ACTS as the n-dimensional set of independently achievable quadrotor thrusts, forming an n-orthotope:

$$\mathcal{H} = \left\{\mathbf{f} \in \mathbb{R}^n : \underline{\mathbf{f}} \leq \mathbf{f} \leq \bar{\mathbf{f}}\right\} \tag{7}$$

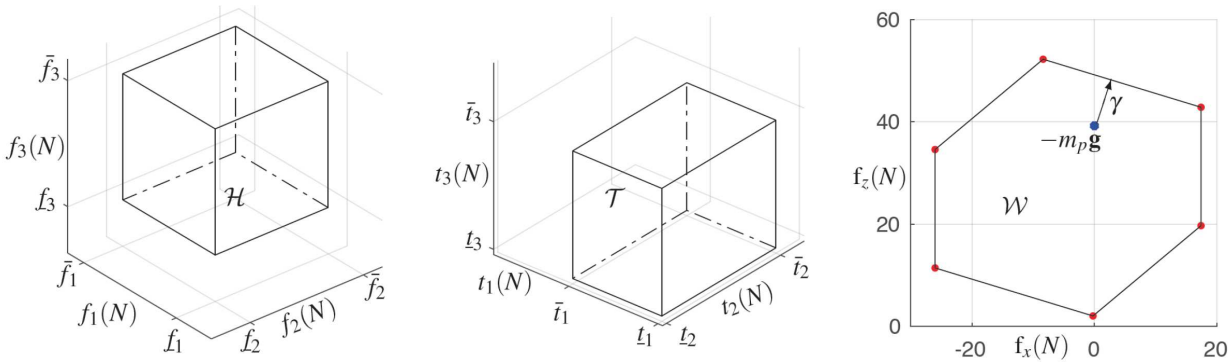

(a) Thrust space (b) Tension space (c) Wrench space

Fig. 5: Thrust $\mathcal{H}$, tension $\mathcal{T}$ and wrench $\mathcal{W}$ spaces of the planar ACTS in Figure 4

where $\mathbf{f} = [f_1, \ldots, f_n]^T$.

4.2 Tension Space

Assumption 3: Cables tensions are always positive, and the projection of every cable on the z axis is positive, i.e., $[0\ 0\ 1]\mathbf{u}_j > 0$.

Tension space is the set of tensions that the quadrotors are able to exert on the cables. Each cable j has tension t_j such that $0 < \underline{t}_j \leq t_j \leq \bar{t}_j$. The minimum tension is chosen such that there will not be excessive sag in the cable [22], and the maximum tension is the maximum force the quadrotor can exert on the cable (assumed to be less than the cable's safe operating tension). Accordingly, the tension space can be generalized as:

$$\mathcal{T} = \{\mathbf{t} \in \mathbb{R}^m : \underline{\mathbf{t}} \leq \mathbf{t} \leq \bar{\mathbf{t}}\} \tag{8}$$

where $\mathbf{t} = [t_1, \ldots, t_m]^T$. As each cable is supported by a quadrotor of finite thrust and non-zero mass, a component of the thrust of the quadrotor must counteract its own weight, with the remainder being available to support the cable tension. The balance of forces for the i^{th} quadrotor in this example is given by Eqn. (9).

$$f_i\mathbf{v}_i + m_i\mathbf{g} - t_i\mathbf{u}_i = m_i\ddot{\mathbf{x}}_i \tag{9}$$

With f_i, t_i and $\mathbf{v}_i$ being unknown, this is an under defined equation. It can be recognized however that the orientation of the quadrotor is controllable, thus $\mathbf{v}_i$ can be eliminated in Eqn. 10 for the purpose of the wrench analysis using its property as a unit vector.

$$f_i^2\mathbf{v}_i^T\mathbf{v}_i = [t_i\mathbf{u}_i + m_i(\ddot{\mathbf{x}}_i - \mathbf{g})]^T[t_i\mathbf{u}_i + m_i(\ddot{\mathbf{x}}_i - \mathbf{g})] \tag{10}$$

This leads to the explicit relationship between tension and thrust in Eqn. 11.

$$t_i^2 + 2t_i m_i\mathbf{u}_i^T(\ddot{\mathbf{x}}_i - \mathbf{g}) + m_i^2(\ddot{\mathbf{x}}_i^T\ddot{\mathbf{x}}_i + \mathbf{g}^T\mathbf{g}) - f_i^2 = 0 \tag{11}$$

It is apparent that the maximum achievable tension must occur at the maximum quadrotor thrust, therefore the maximum tension can be mapped from thrust space to tension space by Eqn. 12.

$$\bar{t}_i = m_i\mathbf{u}_i^T(\mathbf{g} - \ddot{\mathbf{x}}_i) + \sqrt{\bar{f}_i^2 + m_i^2\left(\left(\mathbf{u}_i^T(\ddot{\mathbf{x}}_i - \mathbf{g})\right)^2 - \ddot{\mathbf{x}}_i^T\ddot{\mathbf{x}}_i - \mathbf{g}^T\mathbf{g}\right)} \tag{12}$$

Considering only quasi-static motion, this can be reduced to the expression in Eqn. (13) where $u_{iz} = [0\ 0\ 1]\mathbf{u}_i$ and $g = [0\ 0\ 1]\mathbf{g}$.

$$\bar{t}_i = m_i g u_{iz} + \sqrt{\bar{f}_i^2 + m_i^2 g^2\left(u_{iz}^2 - 1\right)} \tag{13}$$

4.3 Available Wrench Set

The wrench that each cable exerts on the platform can be mapped from tension space to wrench space with the wrench matrix $\mathbf{W}$. The platform is in static equilibrium when $\mathbf{W}\mathbf{t} + \mathbf{w}_e = 0$, where $\mathbf{t} \in \mathcal{T}$ [17, 20].

$$\mathbf{W} = \begin{bmatrix} \mathbf{u}_1 & \cdots & \mathbf{u}_m \\ \mathbf{R}_p\mathbf{b}_1 \times \mathbf{u}_1 & \ldots & \mathbf{R}_p\mathbf{b}_m \times \mathbf{u}_m \end{bmatrix} \tag{14}$$

The wrench space is the set of wrenches that the cables are able to exert on the payload expressed in $\mathcal{F}_0$ as described in Eqn. (15), where $\mathbf{w}_i$ is the i^{th} column of the wrench matrix $\mathbf{W}$ and $\Delta t_i = \bar{t}_i - \underline{t}_i$. A wrench $\mathbf{w}$ is inside the available wrench set if and only if it satisfies Eqn. (15).

$$\mathcal{W} = \left\{\mathbf{w} \in \mathbb{R}^d | \mathbf{w} = \sum_{j=1}^{m} \alpha_j \Delta t_j \mathbf{w}_j + \mathbf{W}\underline{\mathbf{t}}, \quad 0 \leq \alpha_j \leq 1\right\} \tag{15}$$

As the tension space in this example is an orthotope which is necessarily a convex set, the linear mapping of the points bounding the tension space is also a convex set. Therefore the mapping of the vertices of the tension space by the wrench matrix fully and exclusively contains all feasible wrenches. Using the convex hull method described in [21],

the achievable wrench set of the system can be found as the convex hull of the set of d-dimensional points $\mathbf{W}_a$.

$$\mathbf{W}_a = \mathbf{W} diag(\Delta \mathbf{t}) \boldsymbol{\alpha} + \mathbf{W} \underline{\mathbf{t}} \, \mathbf{1}_{(1,2^n)} \tag{16}$$

where $\mathbf{1}_{(1,2^n)}$ is a row vector of ones with 2^n columns. In the planar example considered here, the matrix $\boldsymbol{\alpha}$ is the set of all combinations of tension limits bounding the tension space

$$\boldsymbol{\alpha} = \begin{bmatrix} 0 & 0 & 0 & 0 & 1 & 1 & 1 & 1 \\ 0 & 0 & 1 & 1 & 0 & 0 & 1 & 1 \\ 0 & 1 & 0 & 1 & 0 & 1 & 0 & 1 \end{bmatrix} \tag{17}$$

It is apparent that the mapping from tension space vertices to wrench space generates eight wrenches, however the wrench space in Fig. 5c has six vertices only. That is because, due to the redundant nature of the cable system ($m > d$), two mapped tension vertices are internal to the convex set formed by the other six wrenches.

4.4 Capacity Margin

The capacity margin γ is an index used to evaluate the robustness of equilibrium [16, 20]. It is defined as the shortest distance from the $\mathbf{w}_e$ to the nearest facet of $\mathcal{W}$. Throughout the entirety of the wrench set determination, the orientation of the quadrotor thrust was held to be arbitrary, constrained solely by its maximum magnitude. This leads to the corollary that the capacity margin can be used to determine the minimum set of external wrenches on the platform that the ACTS can compensate for solely with modifications to the attitude of the quadrotor. As the dynamics of the attitude control of quadrotors are much faster than those of the translational control, compensating for disturbances with attitude only should provide a more robust system. In this planar case, the attitude ϕ of the quadrotor results in $\mathbf{v}_i = [sin(\phi), cos(\phi)]^T$, such that Eqn. (9) is satisfied.

5 CASE STUDIES

Several quasi-static case studies are provided to demonstrate the computation of the available wrench set. In the first case, a planar ACTS composed of a rigid platforms with two quadrotors and three cables is analyzed, differing from the previous example through a coupling between two dimensions of the tension space, as well as a non-homogenous wrench space. The study is then extended to two 6-DOF spatial systems, the first of which is a redundantly actuated platform with eight quadrotors and eight cables, the other being a system of three quadrotors and six cable such as is used in [12]. All examples use quadrotors with a mass of $0.8kg$ and a maximum thrust of $32N$.

5.1 Planar System with 2 Quadrotors and 3 Cables

If the object being transported is large, the moments that can be applied to the platform become of greater importance.

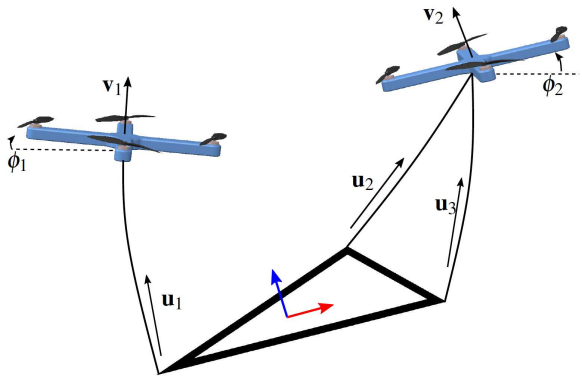

Fig. 6: A planar ACTS with two quadrotors and three cables

Multiple cables attached to a single quadrotor may improve the orientation control of the platform without increasing the number of quadrotors. For the ACTS shown in Fig. (6), the thrust space to tension space mapping of quadrotor 1 to cable 1 can be done using the same methodology as the previous example. The second quadrotor is connected to two cables, and has the equilibrium equation shown in Eqn. (18)

$$f_2 \mathbf{v}_2 + m_2 \mathbf{g} - t_2 \mathbf{u}_2 - t_3 \mathbf{u}_3 = m_p \ddot{\mathbf{x}}_i \tag{18}$$

To determine the tensions in the two cables, there are five controllable variables $(f_2, t_2, t_3, v_{2x}, v_{2z})$. To maintain generality, we consider that cables j and k connect to quadrotor i. This set of equations can be reduced to an equation relating the thrust of the quadrotor to the magnitude of the two cable tensions as was done in Eqn. 10, with the result shown in Eqn. 19.

$$\begin{aligned} t_j^2 + t_k^2 + 2m_i(t_j \mathbf{u}_j^T + t_k \mathbf{u}_k^T)(\ddot{\mathbf{x}}_i - \mathbf{g}) \\ + 2t_j t_k \mathbf{u}_j^T \mathbf{u}_k + m_i^2(\ddot{\mathbf{x}}_i^T \ddot{\mathbf{x}}_i + \mathbf{g}^T \mathbf{g}) - f_i^2 = 0 \end{aligned} \tag{19}$$

By writing Eqn. (19) to solve for t_2 as $t_2 = h_2(t_3, f_2)$ and likewise $t_3 = h_3(t_2, f_2)$ the cable tension space can be formulated as the set of inequalities in Eqn .20.

$$\mathcal{T} = \mathbf{t} \in \mathbb{R}^3 \begin{cases} \underline{t}_1 \le t_1 \le \bar{t}_1 \\ \underline{t}_2 \le t_2 \le h_2(t_3, \bar{f}_2) \\ \underline{t}_3 \le t_3 \le h_3(t_2, \bar{f}_2) \end{cases} \tag{20}$$

The main difference in computing the available wrench set for this system is the $\boldsymbol{\alpha}$ matrix used in Eqn. (16). Appendix A proves that, given the sufficient conditions of cables j and k projecting along the positive $\mathbf{z}_0$ axis, and the angle between cables j and k being less than $\frac{\pi}{2} rad$, the function $t_j = h_j(t_k, \bar{f}_i)$ is convex over the domain $\underline{t}_k \le t_k \le \bar{t}_k$. This property guarantees that the mapping of any set of points in the tension space produces a convex set exclusively containing feasible wrenches. In figure 7(a) six tension space

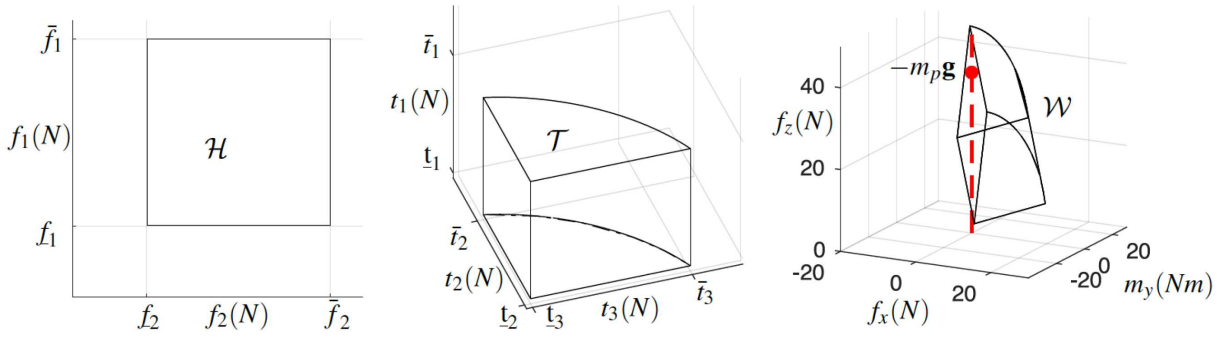

(a) Thrust space (b) Tension space (c) Wrench space

Fig. 7: Thrust, tension and wrench spaces of a planar ACTS with two quadrotors and three cables

vertices are clearly identifiable, however mapping only these points will result in an over conservative set of available wrenches. To approximate the full wrench set, the arc between $\bar{t}_2$ and $\bar{t}_3$ is divided into $p+1$ segments. The combination matrix of the tension span of the second and third cables is denoted as $\boldsymbol{\alpha}_{23}$.

$$\boldsymbol{\alpha} = \begin{bmatrix} \mathbf{0}_{(1,3+p)} & \mathbf{1}_{(1,3+p)} \\ \boldsymbol{\alpha}_{23} & \boldsymbol{\alpha}_{23} \end{bmatrix} \tag{21}$$

The $\boldsymbol{\alpha}_{23}$ matrix includes the three vertices of the t_2, t_3 plane, and a set of vertices evaluated at interpolation points $t_{3,k} = h_3(t_{2,k}, \bar{f}_2)$ for all interpolation points $k \in \mathbb{Z} \mid 1 \leq k \leq p$. The full $\boldsymbol{\alpha}_{23}$ matrix is shown in Eqn. (22).

$$\boldsymbol{\alpha}_{23} = \begin{bmatrix} 0\ 1\ 0 & \frac{k}{p+1} & \cdots & \frac{p}{p+1} \\ 0\ 0\ 1 & \frac{h_3(\frac{k\Delta t_2}{p+1} + \underline{t}_2) - \underline{t}_3}{\Delta t_3} & \cdots & \frac{h_3(\frac{p\Delta t_2}{p+1} + \underline{t}_2) - \underline{t}_3}{\Delta t_3} \end{bmatrix} \tag{22}$$

As the available wrench set of this robot is $\mathbf{w} \in [f_x\ f_z\ m_y]$, it must be homogenized to allow for a calculation of the capacity margin. In [16], the capacity margin is homogenized by dividing the moment by the radius of gyration $r_g = \sqrt{I/A}$ of the platform, where A is the area of the platform and I is the second area moment of inertia. If $\mathbf{W}_a$ is the matrix whose columns form a set of points bounding the convex wrench space, the homogenized wrench space boundary is given by Eqn. (23).

$$\mathbf{W}_h = \begin{bmatrix} \mathbb{I}_2 & 0 \\ 0 & \frac{1}{r_g} \end{bmatrix} \mathbf{W}_a \tag{23}$$

where $\mathbb{I}_2$ is an identity matrix of rank 2. In this case study the system parameters are defined as: $\mathbf{R} = \mathbf{R}_y(\pi/6)$ where $\mathbf{R}_y(x)$ is the rotation matrix about $\mathbf{y}_0$ by angle x, platform mass $m_p = 4kg$, platform dimensions $\mathbf{b}_1 = [-0.75\ -0.25]^T$ m, $\mathbf{b}_2 = [0.5\ 0.5]^T$ m, $\mathbf{b}_3 = [1.0\ -0.25]^T$ m, cables of 0.75 m in length, and $\mathbf{u}_1 = [0\ 0\ 1]^T$. Fig. 7(c) shows the available wrench set, with the dotted line indicating the line

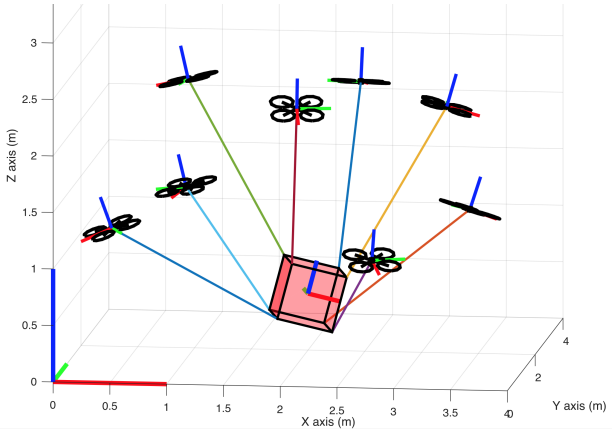

Fig. 8: A 6-DOF ACTS with a cubic payload, eight quadrotors and eight cables

of action of $\mathbf{w}_e$. The capacity margin of the ACTS in this configuration is 0.3N, so this configuration is on the border of equilibrium. It is noteworthy that solely reducing m_p here does little to change γ, but that γ increases significantly with a combination of $\mathbf{w}_e = [0\ 0\ -m_y]$ and decreased m_p. The attitudes ϕ_1 and ϕ_2 of the quadrotors are chosen such that for the point in tension space $\mathbf{t} = \mathbf{W}^{-1}(m_p\mathbf{g} - \mathbf{w}_e)$, Eqn. (9) is satisfied for the first quadrotor, and Eqn. (18) is satisfied for the second quadrotor.

5.2 Spatial System with 8 Quadrotors and 8 Cables

In this case, the platform is desired to have a controllable orientation without holonomic constraints on the twist. The ACTS, shown in Fig. (8) has a cubic moving platform with side lengths of 0.5 m, mass $m_p = 4$ kg, and orientation of $\mathbf{R} = \mathbf{R}_{xyz}(\frac{\pi}{12}\ \frac{\pi}{12}\ 0)$. It is manipulated by eight quadrotors so that all twists are independently achievable with two degrees of actuation redundancy in non-singular states. A configuration has been chosen to avoid singularities for the evaluation of the available wrench set. The vector $\mathbf{u}_i$ of the cables connected to the lower vertices of the platform are rotated by $\frac{-\pi}{6} rad$ from the direction of $\mathbf{b}_i$ about $\mathbf{z}_0$, and then given an elevation of $\frac{\pi}{6} rad$ from the xy-plane. The upper cables are

Table 1: Thrust and tension space limits for the eight quadrotors, eight cables case study shown in figure 8

Quadrotor	$\underline{f}(N)$	$\bar{f}(N)$	Cable	$\underline{t}(N)$	$\bar{t}(N)$
1	8.7	32.0	1	1.0	25.0
2	8.4	32.0	2	1.0	27.4
3	8.7	32.0	3	1.0	25.0
4	8.4	32.0	4	1.0	27.4
5	8.7	32.0	5	1.0	25.0
6	8.4	32.0	6	1.0	27.4
7	8.7	32.0	7	1.0	25.0
8	8.4	32.0	8	1.0	27.4

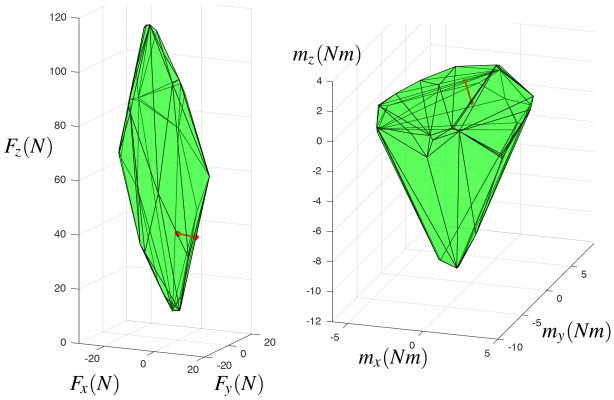

Fig. 9: Achievable wrench space of the eight quadrotor, eight cable ACTS evaluated at $\mathbf{w}_{moment} = [0\,0\,0]^T$ Nm (left) and at $\mathbf{w}_{force} = m_p\mathbf{g}$ N (right).

rotated in the opposite direction by $\frac{\pi}{6}rad$ from $\mathbf{b}_i$ about $\mathbf{z}_0$, and then elevated by $\frac{\pi}{3}rad$ from the xy-plane.

In this case, the thrust space is computed for each quadrotor as in the previous section, resulting in a 8-orthotope. The tension space is likewise calculated to result in an 8-orthotope using Eqn. (11). The result is the same as in the planar system, with the thrust space to tension space mapping being described by Eqn. (13). The vertices of the thrust and tension spaces are combinations of maximum and minimum thrust and tension values in Table (1).

Mapping the vertices of the tension space orthotope to task space results in a convex 6-zonotope [18, 21] bounding the available wrench set of the ACTS. Fig. (9) shows the available wrench set evaluated at $\mathbf{m}_e = 0$ (left) and at $\mathbf{f}_e = -m_p\mathbf{g}$ (right). From this, it is seen that the system can exert a force wrench between 10N and 120N along $\mathbf{z}_0$, and forces between -20N and 20N laterally, with the largest lateral wrench range occuring when the vertical force is around 60N. This ACTS has little ability to withstand positive moments about $\mathbf{z}_0$ limiting the capacity margin to $\gamma = 6.5N$. This ACTS configuration would be useful in situations that required (primarily vertical) movements, as well as roll and pitch capabilities, but without strict yaw requirements.

While the wrench feasibility can be quantified using the capacity margin after normalizing $\mathbf{W}_a$ by Eqn. (24), the configuration of this particular ACTS does not lend itself well toward numerical optimization, as the set of variables (the altitude and azimuth of each cable) is 16 dimensional. Intuitive configurations avoiding common singularities can however, be evaluated for their robustness.

$$\mathbf{W}_h = \begin{bmatrix} \mathbb{I}_3 & 0 \\ 0 & \frac{\mathbb{I}_3}{r_g} \end{bmatrix} \mathbf{W}_a \tag{24}$$

The attitude of the quadrotors must be controlled so as to choose $\mathbf{v}_i$ satisfying $f_i\mathbf{v}_i + m_i\mathbf{g} - t_i\mathbf{u}_i = 0$. As the system is redundant in this case, using the Moore-Pensrose pseudo-inverse of $\mathbf{W}$ finds the least norm vector of cable tensions that will maintain equilibrium. This may result in negative tensions, however the inclusion of $\mathbf{w}_e$ within $\mathcal{W}$ guarantees a set of continuous feasible tensions satisfying the dynamic equilibrium of the ACTS to exist [18]. Tension $\mathbf{t} \in \mathcal{T}$ (when $m > d$) can be found though adding a projection of the null space of $\mathbf{W}$ by a scalar factor $\boldsymbol{\lambda} = [\lambda_1 \cdots \lambda_{m-d}]$ onto the least norm solution of the tensions (as in Eqn. (25) in order to satisfy properties such as continuity, least maximum tension, or other criteria. Tension distribution algorithms to determine $\boldsymbol{\lambda}$ are well studied in the domain of CDPR control and the reader is referred to [23, 24] for greater details.

$$\mathbf{t} = \mathbf{W}^{\dagger}(\mathbf{w_e} - m_p\mathbf{g}) + \mathbf{N}\boldsymbol{\lambda}, \text{ where } \mathbf{N} = null(\mathbf{W}) \tag{25}$$

The rotation matrix of each quadrotor is under-constrained by 1-DOF, as the rotation of the i^{th} quadrotor around $\mathbf{v}_i$ has no effect on the system equilibrium [25], and any rotation matrix of the under-constrained quadrotor may be chosen so long as the equation $\mathbf{R}_i[0\,0\,1]^T = \mathbf{v}_i$ is satisfied.

5.3 Spatial System with 3 Quadrotors and 6 Cables

The Flycrane ACTS has been studied for motion planning in [12], and is composed of three quadrotors and six cables. A benefit of this design is the ability to generate six independent wrenches using only three quadrotors. It also has the advantage of being significantly easier to optimize, with a three dimensional configuration space compared to the 16 dimensional configuration space in the previous case.

The ACTS in this case is displayed in Fig. (10). platform orientation is $\mathbf{R} = \mathbf{R}_{xyz}(\frac{\pi}{12}\ \frac{\pi}{12}\ 0)$ and $m_p = 4kg$. The platform is parameterized as $\mathbf{b}_i = 0.5\left[cos\left(\frac{2\pi i}{6}\right)\ sin\left(\frac{2\pi i}{6}\right)\ 0\right]$ m, $i \in \mathbb{Z}, 1 \leq i \leq 6$. The cable pairs have lengths of $L_{1,2} = 0.35m$, $L_{3,4} = 0.70m$, and $L_{5,6} = 1.40m$. Each quadrotor is at an inclination of $\frac{\pi}{4}rad$ from the $\mathbf{z}_p$ axis.

The 3-orthotope thrust space is mapped to the 6-dimensional cable tension space, with the tension in each pair of cables (j and k) being related to the thrust of a single quadrotor (i) through Eqn. (26).

$$f_i\mathbf{v}_i + m_i\mathbf{g} - t_j\mathbf{u}_j - t_k\mathbf{u}_k = 0 \tag{26}$$

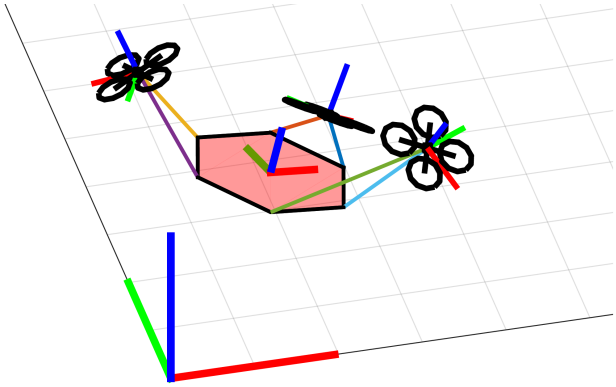

Fig. 10: Diagram of the Flycrane ACTS with non-homogeneous cable lengths

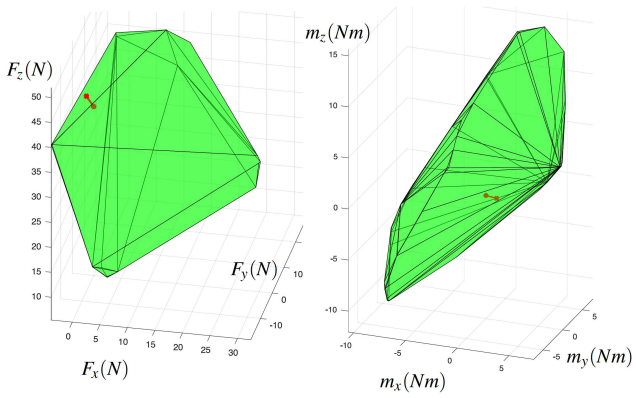

Fig. 11: Available wrench set of the Flycrane evaluated at $\mathbf{w}_{moment} = [0\ 0\ 0]^T$ Nm (left) and at $\mathbf{w}_{force} = m_p\mathbf{g}$ N (right).

Table 2: Thrust and tension space limits for the Flycrane ACTS case study. As the maximum tension of cables j and k connected to quadrotor i are coupled, $\bar{t}_j$ is evaluated at its maximum value of $\bar{t}_j = h_j(\underline{t}_k, \bar{f}_i)$

Quadrotor	$\underline{f}(N)$	$\bar{f}(N)$	Cable	$\underline{t}(N)$	$\bar{t}(N)$
1	8.6	32.0	1	1.0	27.6
			2	1.0	28.8
2	9.5	32.0	3	1.0	24.4
			4	1.0	24.9
3	9.3	32.0	5	1.0	25.5
			6	1.0	25.0

To determine the tensions in the two cables, there are 6 variables $(t_j, t_k, f_i, v_{ix}, v_{iy}, v_{iz})$. An additional equation is found as $\mathbf{v}_i$ is a unit vector, resulting in 4 equations with 6 unknowns. Considering quasi-static motion reduces to Eqn. (19), generalized in Eqn. (27) for cables j and k.

$$t_j^2 + t_k^2 + 2t_j t_k \left(\mathbf{u}_j^T \mathbf{u}_k\right) - 2m_i g(t_j u_{jz} + t_k u_{kz}) + m_i^2 g^2 - f_i^2 = 0 \quad (27)$$

Each of the three orthogonal 2-dimensional tension space components, which are all composed of straight lines along the lower bound tensions, and the upper bound tension is described by an analytic function h, where $t_j = h_j(t_k, \bar{f}_i)$, creating a 6 dimensional solid composed of a combination of flat and curved surfaces. It can be seen on the $t_j t_k$-plane that for longer cables ($\mathbf{u}_j^T \mathbf{u}_k \approx 1$), the upper bound of the curve approaches a straight line joining the vertices $\left(\underline{t}_j, h_k(\underline{t}_j, \bar{f}_i)\right)$ and $\left(h_j(\underline{t}_k, \bar{f}_i), \underline{t}_k\right)$. As the number of interpolation points p along the curve $t_j = h_j(t_k, \bar{f}_i)$ increases, the size of the convex set of points increases by the cube of the number of points $(3+p)^3$. Short cables relative to the baseline separating the cables increases the curvature of the maximum tension curve, increasing the importance of interpolations. The vertices of the thrust space and the cable tension space are shown in Table (2). In the same manner as is done for the planar system with two quadrotors and three cables, the available wrench space of this ACTS can be mapped through interpolated vertices along the convex curved surfaces. The combination matrix $\boldsymbol{\alpha}$ is built as all combinations of the columns of $\boldsymbol{\alpha}_{jk}$, derived as in Eqn. (22), and arranged as shown in Eqn. (28)

$$\boldsymbol{\alpha} = comb\left(\begin{bmatrix}\boldsymbol{\alpha}_{12}\\ \boldsymbol{\alpha}_{34}\\ \boldsymbol{\alpha}_{56}\end{bmatrix}\right) \quad (28)$$

The available wrench set of the ACTS is shown in Fig. (11). The ACTS in this configuration can apply a peak force of 50N along $\mathbf{z}_0$, and a peak force of 30N in the positive $\mathbf{x}_0$ direction, however it can only exert a force of 2N along the negative $\mathbf{x}_0$ axis. It is able to exert moments from -10 Nm to 15 Nm about $\mathbf{z}_0$, but much less around $\mathbf{x}_0$ and $\mathbf{y}_0$.

5.4 Remarks on the Computational Complexity

The method presented in this paper is capable of performing an analysis of varied ACTS architectures. However there are practical limitations such as computational complexity. The number of tension space to wrench space mappings is given by $2^{n1}(3+p)^{n2}$ where $n1$ is the number of quadrotors with one cable and $n2$ is the number with two cables. With a large number of wrench vertices, the determination of the convex hull as well as the the inclusion of $\mathbf{w}_e$ within $\mathcal{W}$ becomes computationally expensive.

Another issue arising in the application of this methodology for solving optimal configuration problems is the size of the configuration space which varies by the design of the ACTS. The eight-quadrotor, eight-cable ACTS (ACTS-8) and the Flycrane each have 6-DOF freedom platforms, however ACTS-8 has configuration $\mathcal{C} \in \mathbb{R}^{16}$, while the Flycrane has configuration $\mathcal{C} \in \mathbb{R}^3$. As the capacity margin γ is continuous (assuming a continuous $\mathbf{w}_e$), gradient descent methods may be used to optimize the configuration, but in the case of ACTS-8, the size of the configuration space is still

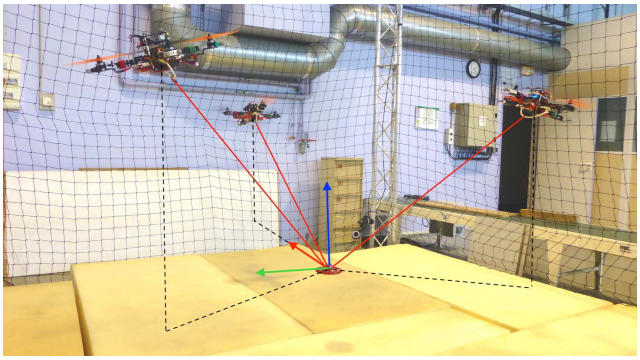

Fig. 12: ACTS prototype developed at LS2N

problematic. With such a large system, it becomes important to use heuristic parameterization to reduce the problem to a reasonable size. This can include forcing symmetry around the $\mathbf{w}_e$ axis, and using knowledge of mechanics to avoid singularities. In the case study provided for the ACTS-8, the configuration space is parameterized in $\mathbb{R}^4$, with the cables being divided into two groups, and cable j in group g being parameterized by azimuth and elevation angles (ϕ_g, θ_g) with respect to the projection of $\mathbf{b}_j$ on the plane normal to $\mathbf{w}_e$.

Even with simplifying assumptions, it is unlikely to be applicable to real-time configuration planning for the ACTS-8, but more appropriate uses would be the optimization of pre-planned tasks or motions, as well as the optimal design of the system. This could include the location of the cable connection points, or in the case of coupled cables, the cable lengths. For systems such as the Flycrane in which $\mathcal{C} \in \mathbb{R}^3$, a real-time optimization of C to maximize γ during motion planning could potentially be feasible but hasn't yet be attempted.

6 EXPERIMENTAL VALIDATION

An ACTS prototype composed of three quadrotors connected to a point mass payload moving in 3D cartesian space was constructed at LS2N. The configuration $\mathcal{C}$ is the set of all cable directions decomposed into an azimuth ϕ_i (angle of rotation about $\mathbf{z}_0$) and inclination θ_i (angle from $\mathbf{z}_0$ to the cable) for each cable. With the control methodology being outside the scope of this paper (but similar to [10]), it is sufficient to know that the state is composed of the payload position $\mathbf{x}_p$, velocity $\dot{\mathbf{x}}_p$, and the configuration $\mathcal{C}$ and $\dot{\mathcal{C}}$.

Each quadrotor has a mass $m_i = 1.05$ kg, and a maximum thrust $\bar{f}_i = 18.0$ N. They were built using a Lynxmotion Crazy2fly frame, 8"x4.5" ABS propellors, a Pixhawk flight control unit, and a Raspberry Pi 3B as an onboard computer. Quadrotor and payload position feedback was provided by a Qualysis motion capture system with 1mm precision. The cables are connected to the quadrotors throught a passive spherical mechanism ensuring the offset between the tension line of action and the geometric center of the quadrotor to be lower than 7mm regardless of orientation. The cables used were 0.5mm braided PE line with a measured linear density of 0.2 g/m and an elongation factor of 0.05 %/N. With cables of 1.3 m in length and tensions ranging from 1-10 N, the effects of cable elongation and sag on the experiments are negligible compared to other factors such as uncertainty in the applied thrust and communication delays in the controller.

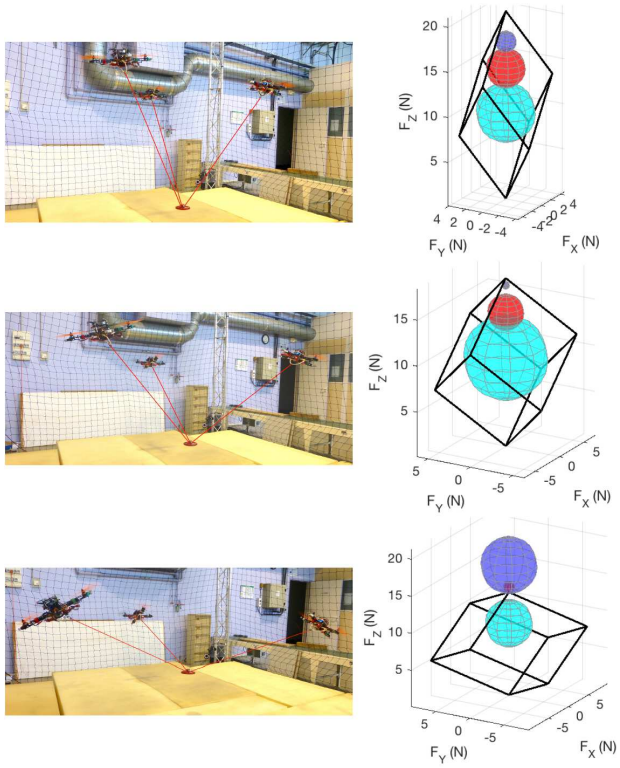

Fig. 13: The available wrench set of the ACTS prototype at $\theta = 35^o$ (top), 50^o (middle) and 65^o (bottom) under quasi-static motion. The cyan, red and blue spheres are centred at $\mathbf{w}_e = -m_p\mathbf{g}$ for payload masses of 1.0 kg, 1.5 kg and 1.8 kg respectively and have radius corresponding to the magnitude of their respective capacity margins.

To validate the wrench analysis, the ACTS tracked a quasi-static trajectory $\mathbf{x}_p^d(t)$, during which $||\ddot{\mathbf{x}}_p^d|| < 0.06\ \mathrm{ms}^{-2}$ and the external wrench is $\mathbf{w}_e = m_p\mathbf{g}$. External wrench forces in the xy-plane could be tested with modifications to the controller. The testing capability of the ACTS to resist external moments would require a rigid body payload and may be investigated in the future. The desired configuration is $\mathcal{C}^d(t) = [\boldsymbol{\phi}^d\ \boldsymbol{\theta}^d]$ where $\boldsymbol{\phi}^d = [0\ 120\ -120]^o$, $\boldsymbol{\theta}^d(t) = [\theta^d(t)\ \theta^d(t)\ \theta^d(t)]^o$. The desired inclination angle θ^d began at 35^o, and was increased at a rate of $1.5^o/s$ to modify $\mathcal{W}$. For instance, Fig. 13 shows the available wrench sets of the ACTS for different payload masses and configurations. The configuration at which the ACTS diverged from the trajectory ($||\mathbf{x}_p - \mathbf{x}_p^d||$ becomes unbounded) is considered to be the limit of wrench feasibility.

The capacity margin of the symmetric ACTS is plotted as a function of θ^d in Fig 14 while the position tracking error is plotted as a function of the mean value of $[\theta_1\ \theta_2\ \theta_3]$. The results show a good correlation between the estimated unstable configuration based on γ and the configuration at

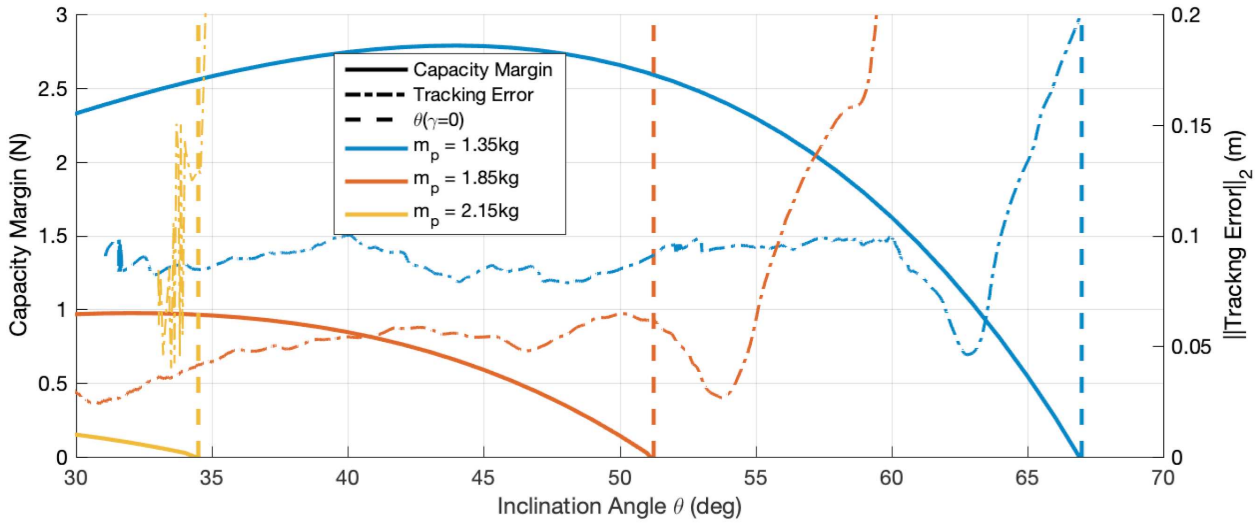

Fig. 14: The capacity margin γ (solid lines), and the 2-norm of the platform position tracking error (dot-dashed lines) as a function of the mean angle θ. The error is bounded within the set of positive γ, and diverges when $\gamma \approx 0$.

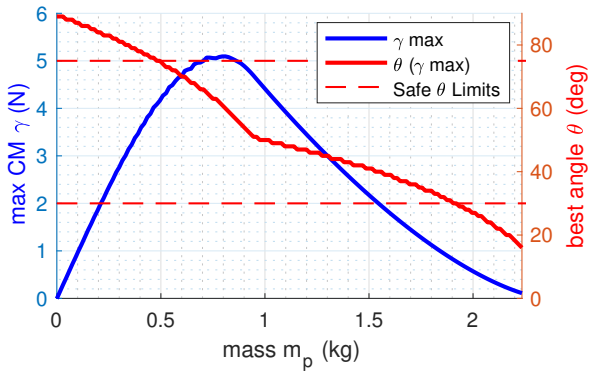

Fig. 15: Plot of the capacity margin (blue), and the inclination angle (red) at which it occurs as a function of the payload mass for the ACTS prototype in quasi-static motion

which the ACTS crashed. Table 3 shows for various payload masses, the maximum capacity margin $\bar{\gamma}$, the predicted mean $\boldsymbol{\theta}^d$ value of zero capacity margin θ ($\gamma = 0$), the actual mean $\boldsymbol{\theta}$ value at the time of loss of control θ_{crash}, and the difference between predicted and actual unstable configurations. With each configuration being controlled to an accuracy of ±5 deg, all tests but one ($m_p = 2.05$ kg, possibly an error in experimental procedure) are within the bounds of error for crashing at the point of zero capacity margin. With a tracking error generally ranging from 5-10 cm, it can be difficult to determine when the instability actually began, so θ_{crash} is taken as the configuration at which the tracking error diverged beyond 0.1 m. A video of some experiments[1] shows a clear correspondence between the configuration with $\gamma = 0$ N, and the ability of the ACTS to follow trajectories.

Figure 15 shows the evolution of the maximum capacity margin $\bar{\gamma}$ and the configuration at which the maximum capacity occurs as a function of the payload mass. Limits are

[1]The video can be found at `https://youtu.be/UipyUgF82ZY`

Table 3: Comparison of the mean θ when the ACTS crashed (error diverges > 0.1 m) to the predicted configuration limit of θ ($\gamma = 0$ N)

Mass	(kg)	1.15	1.35	1.65	1.85	2.05	2.15
$\bar{\gamma}$	(N)	3.7	2.8	1.6	1.0	0.5	0.25
θ ($\gamma = 0$)	(deg)	71	67	58	51	40	34
θ_{crash}	(deg)	70	64	60	56	50	34
Error	(deg)	1	2	-2	-4	10	-1

imposed on the safe range of θ, with the lower limit being chosen to keep the quadrotors a safe distance apart and the upper limit being chosen to maintain a safe distance from actuation singularities in the controller, occurring when all cables are co-plannar.

7 DYNAMIC WRENCH ANALYSIS

The previous case studies showed how the proposed methodology can be applied to any reconfigurable ACTS with quasi-static quadrotor motion. This section shows the effect of considering the dynamics for the experimental ACTS at a constant configuration displayed in Fig. 12. At a constant configuration, acceleration of the payload and quadrotors are the same, thus the system acceleration will be described by $\ddot{\mathbf{x}}_p$. As there is an explicit second order kinematic relationship between the state acceleration $\ddot{\mathbf{x}}_p, \ddot{C}$ and the quadrotors accelerations $\ddot{\mathbf{x}}_1, \ddot{\mathbf{x}}_2, \ddot{\mathbf{x}}_3$, this methodology can be easily adapted for time-varying ACTS configurations as well.

Figure 16 shows the effects of different magnitudes and directions of acceleration for the ACTS pictured in Fig. 12 at a constant configuration of $\boldsymbol{\phi} = [0\ \frac{2\pi}{3}\ \frac{-2\pi}{3}]$, $\boldsymbol{\theta} = [\frac{\pi}{4}\ \frac{\pi}{4}\ \frac{\pi}{4}]$, and a payload mass of $m_p = 1.15$ kg. There is a marked

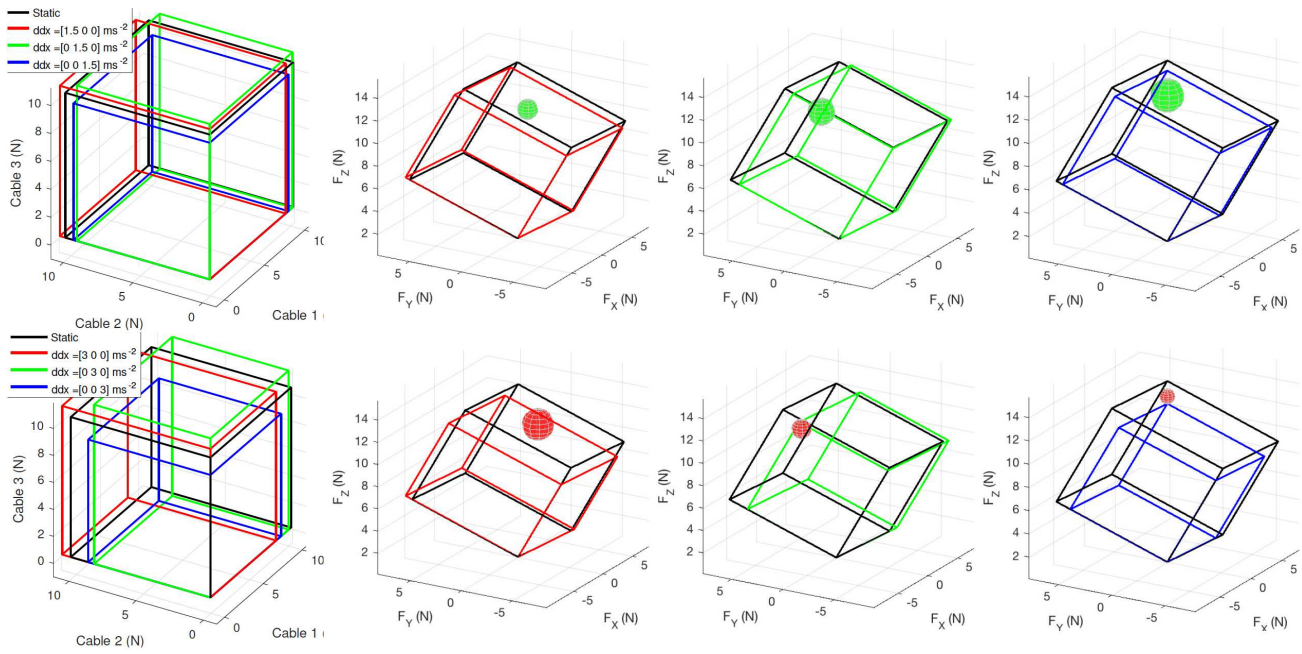

Fig. 16: Dynamic wrench analysis for linear accelerations along X (red), Y (green) and Z (blue) directions compared to the static result (black). The sphere is centered at $\mathbf{w}_e = m_p(\ddot{\mathbf{x}}_p - \mathbf{g})$ and is tangent to the nearest border of the dynamic available wrench set, thus have a radius of $||\gamma||$. If $\gamma > 0$ N, the sphere is shown in green, otherwise it is red. The leftmost figures shows the tension spaces. The top row has accelerations of magnitude $||\ddot{\mathbf{x}}_p|| = 1.5$ ms^{-2}, and the bottom of $||\ddot{\mathbf{x}}_p|| = 3$ ms^{-2}.

difference in the capacity margin as a function of both the direction and magnitude of the applied acceleration to the system. Despite this, all the scenarios tested fall within the bounds of the static wrench feasibility. This highlights the need to account for dynamics within the wrench analysis, even for accelerations lower than 1 ms^{-2}

Experimental validation of the dynamic wrench analysis may be undertaken at LS2N once the drone arena is expanded to allow sufficient space for dynamic tests.

8 CONCLUSIONS AND FUTURE WORK

In this paper, it is shown how the available wrench set of the payload of an aerial cable towed system (ACTS) can be calculated. This method is adaptable to systems where two cables are coupled due to sharing the actuation of a single quadrotor. It is proven that the relationship between tensions in such a coupled system is necessarily convex given certain operational and design conditions, showing that the available wrench set obtained from a mapping of the tension space is guaranteed to be conservative throughout the wrench space.

From a practical point of view, this has applications in the optimal design and motion planning of ACTS with the objective of increasing the ability to resist external wrenches acting on the moving platform. As the available wrench set is determined through a mapping of the full achievable tension space of the system, it can be seen that the position of the platform and the configuration of the system can be maintained through re-orientation of the thrust vectors while the external wrench is within the bounds of the available wrench set. This can be done through attitude control of the quadrotor, requiring no change in the quadrotors positions. The higher dynamic response of attitude control compared to position control may lead to improvements in response time to system disturbances lying within the available wrench set.

Further investigation of this wrench analysis methodology is underway, with the intention of designing an ACTS optimally suited to exerting desired wrenches on the environment.

References

[1] Kumar, V., and Michael, N., 2012. "Opportunities and challenges with autonomous micro aerial vehicles". *The International Journal of Robotics Research,* ***31***(11), August, pp. 1279–1291.

[2] Tagliabue, A., Kamel, M., Verling, S., Siegwart, R., and Nieto, J., 2017. "Collaborative transportation using mavs via passive force control". In Proceedings of the Int. Conf. on Robotics and Automation.

[3] Tognon, M., and Franchi, A., 2017. "Dynamics, control, and estimation for aerial robots tethered by cables or bars". *IEEE Transaction on Robotics,* ***33***(4).

[4] Gassner, M., Cieslewski, T., and Scaramuzza, D., 2017. "Dynamic collaboration without communication: Vision-based cable-suspended load transport with two quadrotors". In IEEE International Conference on Robotics and Automation (ICRA).

[5] Lee, T., Leoky, M., and McClamroch, N. H., 2010. "Geometric tracking control of a quadrotor UAV on se(3)". In Proceedings of the 49th IEEE Conf. on Decision and Control.

[6] Ruggiero, F., Lippiello, V., and Ollero, A., 2018. "Aerial manipulation: A literature review". *IEEE Robotics and Automation Letters,* ***3***(3).

[7] Khamseh, H., Janabi-Sharifi, F., and Abdessameud, A., 2018. "Aerial manipulation: A literature survey". *Robotics and Autonomous Systems,* ***107***.

[8] Palunko, I., Cruzm, P., and Fierro, R., 2012. "Agile load transport: Safe and efficient load manipulation with aerial robots". *IEEE Robotaics and Automation Magazine,* ***19***(3).

[9] Sreenath, K., and Kumar, V., 2013. "Dynamics, control and planning for cooperative manipulation of payloads suspended by cables from multiple quadrotor robots". In Robotics: Science and Systems.

[10] Masone, C., Bülthoff, H., and Stegagno, P., 2016. "Cooperative transportation of a payload using quadrotors: a reconfigurable cable-driven parallel robot". In IEEE Int. Conf. on Intelligent Robots and Systems.

[11] Alothman, Y., Guo, M., and Gu, D., 2017. "Using iterative LQR to control two quadrotors transporting a cable-suspended load". *International Federation of Automatic Control IFAC-papers online,* ***50***, July.

[12] Manubens, M., Devaurs, D., Ros, L., and Cortes, J., 2013. "Motion planning for 6-d manipulation with aerial towed-cable systems.". In Robotics: Science and Systems, p. 8.

[13] Tognon, M., Gabellieri, C., Pallottino, L., and Franchi, A., 2018. "Aerial co-manipulation with cables: The role of internal force for equilibria, stability, and passivity". *IEEE Robotics and Automation Letters,* ***3***(3).

[14] Gabellieri, C., Tognon, M., Pallottino, L., and Franchi, A., 2018. "A study on force-based collaboration in flying swarms". In Proceedings of the 11th International Conference on Swarm Intelligence.

[15] Bosscher, P., Riechel, A., and Ebert-Uphoff, I., 2006. "Wrench-feasible workspace generation for cable-driven robots". In IEEE Transaction on Robotics, Vol. 22.

[16] Gagliardini, L., Caro, S., Gouttefarde, M., and Girin, A., 2016. "Discrete reconfiguration planning for cable-driven parallel robots". *Mechanism and Machine Theory,* ***100***.

[17] Azizian, K., and Cardou, P., 2013. "The dimensional synthesis of spatial cable-driven parallel mechanisms". *Journal of Mechanisms and Robotics,* ***5***(4), November.

[18] Gosselin, C., 2014. "Cable-driven parallel mechanisms: State of the art and perspectives". *Bulletin of the Japan Society of Mechanical Engineers*.

[19] Michael, N., Fink, J., and Kumar, V., 2011. "Cooperative manipulation and transportation with aerial robots". *Autonomous Robots,* ***30***.

[20] Cruz Ruiz, A. L., Caro, S., Cardou, P., and Guay, F., 2015. "Arachnis: Analysis of robots actuated by cables with handy and neat interface software". *Mechanisms and Machine Science,* ***32***.

[21] Bouchard, S., Gosselin, C., and Moore, B., 2010. "On the ability of a cable-driven robot to generate a prescibed set of wrenches". *ASME Journal of Mechanisms and Robotics,* ***2***(1).

[22] Yuan, H., Courteille, E., and Deblaise, D., 2016. "Force distribution with pose-dependent force boundaries for redundantly actuated cable-driven parallel robots". *Journal of Mechanisms and Robotics,* ***8***(4).

[23] Lamaury, J., and Gouttefarde, M., 2013. "A tension distribution method with improved computational efficiency". In *Cable-Driven Parallel Robots. Mechanisms and Machine Science*, T. Bruckmann and A. Pott, eds., Vol. 12. Springer, Berlin, Heidelberg.

[24] Gosselin, C., and Grenier, M., 2011. "On the determination of the force distribution in overconstrained cable-driven parallel mechanisms". *Meccanica,* ***46***(1).

[25] Lee, T., Sreenath, K., and Kumar, V., 2013. "Geometric control of cooperating multiple quadrotor UAVs with a suspended payload". In Proceedings of the 52nd IEEE Conference on Decision and Control, IEEE.

Appendix A: Proof of Convex Tension Space

This appendix proves that the function relating the maximum tensions of two cables i, j connected to quadrotor Q forms a convex tension space when $\ddot{\mathbf{x}}_i = [0\,0\,0]^T \forall i$. Equation 19 can be rewritten as

$$\bar{t}_i^2 + \bar{t}_j^2 + k_1\bar{t}_i\bar{t}_j + k_2\bar{t}_i + k_3\bar{t}_j + c \quad | \quad 0 < \underline{t} \leq \bar{t} \leq \bar{t}_{max} \tag{29}$$

where $k_1 = \mathbf{u}_i^T\mathbf{u}_j$, $k_2 = -2m_Q g u_{iz}$, $k_3 = -2m_Q g u_{jz}$, and $c = m_Q^2 g^2 - \bar{f}_Q^2$

The maximum tension of cable j, $\bar{t}_j$ relates to $\bar{t}_i$ through the function $t_j = h_j(t_i, f_Q)$, with $\bar{t}_j = h_j\left(\underline{t}_i, \bar{f}_Q\right)$. The function is convex if, over the span of allowable tensions, it can be shown that $\frac{d\bar{t}_j}{dt_i} \leq 0$ and that $\frac{d^2\bar{t}_j}{dt_i^2} \leq 0$ (sufficient conditions, not necessary). Using implicit differentiation, it can be found that the derivative of $\bar{t}_j$ with respect to t_i is

$$\frac{d\bar{t}_j}{dt_i} = -\frac{2\bar{t}_j + k_1 t_i + k_2}{2t_i + k_1\bar{t}_j + k_3} \tag{30}$$

Assuming that the payload is suspended, u_z is positive for all cables, therefore k_2 and k_3 are both positive. Applying a simple design rule $\sqrt{l_i^2 + l_j^2} \geq \|B_j - B_i\|$ forces $0 \leq k_1 \leq 1$. With strictly positive tensions, and $k_1, k_2, k_3 \geq 0$, $\frac{d\bar{t}_j}{dt_i}$ is strictly negative.

By setting $\frac{d\bar{t}_j}{dt_i} = -\frac{g}{h}$, the quotient rule and the law of implicit differentiation can be used to solve the second derivative.

$$\frac{d^2\bar{t}_j}{dt_i^2} = -\frac{g\left(\frac{g}{h} - k_1\right) + h}{h^2} < 0 \tag{31}$$

It is therefore shown that within the domain of $\underline{t}_i \leq t_i \leq \bar{t}_i \forall i$, given that all cable vectors have a positive projection along the z-axis, and that the angle between two cables connected a quadrotor is acute, the tension space is a convex shape.